The study of an integrated sensor for partial nucleate pool boiling at low heat flux

JIANG WenJing, LI ZhiGang, ZHAO JianFu, DU WangFang & YUAN HongTao

Abstract—To study local convention and heat transfer around an isolated growing vapor bubble during nucleate pool boiling on a well characterized flat surface in microgravity, a MEMS sensor has been fabricated to pulse a single bubble boiling. In this paper, we present the design and fabrication process of a MEMS microchip, which can excite a bubble nucleus with accurate spatial and temporal positioning on the top-side of the microchip, and meanwhile, the temperature on the heating surface around and underneath the growing bubble can be measured. The key points and difficulties of chip fabrication have been discussed, including the characteristics of the ultra-thin Ti/Pt (10nm/35nm) film such as the effect of annealing on resistivity, its TCR (temperature coefficient of resistance) and so on. And then the thermal cycling experiment has verified its stability. The results of the preliminary ground tests of the flight module SOBER-SJ10 show the microchip works well as expected, and laid a good foundation for meeting the requirements of future space experiments.

Index Terms—partial nucleate pool boiling, MEMS microchip, micro-heater, micro-RTD, Ti/Pt film

I. INTRODUCTION

With the rapid development of MEMS technology, the application of microheaters has been widely extensive, such as light source, pressure sensors, flow rate sensors, TEM/SEM test chip, micro explosive boiling, and ignition of micro-propulsion systems [1-10]. Since a thin film microheater has lower heat mass, fast response, good heat confinement, good mechanical stability, ease of integration and compatibility with other MEMS sensors. For example, MEMS infrared light source can be used in infrared gas detectors, target identification devices, providing technical support for personnel search and rescue, industrial and mining safety production [1-2]. Devices based on micro explosive boiling have been used in thermal bubble jet printers, biology, space exploration, and microelectronic

JIANG WenJing is with Institute of Microelectronics of The Chinese Academy of Sciences, Beijing, CO100029, China (e-mail: jiangwenjing@ime.ac.cn).

LI ZhiGang is with Institute of Microelectronics of The Chinese Academy of Sciences, Beijing, CO100029, China (e-mail: lizhigang2@ime.ac.cn, Corresponding author).

ZHAO JianFu is with Key Laboratory of Microgravity/CAS, Institute of Mechanics, Chinese Academy of Sciences, Beijing CO100190, China (e-mail: jfzhao@imech.ac.cn).

DU WangFang is with Key Laboratory of Microgravity/CAS, Institute of Mechanics, Chinese Academy of Sciences, Beijing CO100190, China (e-mail: duwangfang@imech.ac.cn).

YUAN HongTao is with Beijing Institute of Nanoenergy and Nanosystems, Chinese Academy of Sciences, Beijing CO101400, China (e-mail: yuanhongtao@binn.cas.cn).

cooling [3-4]. Micro-propulsion systems are also essential in micro-spacecraft, which can be applied for attitude control, delta-v manoeuvring, station keeping, and orbit adjustment [5-6]. In the future they can also provide more interesting solutions for various applications, such as safety and quality control in healthcare and industrial processes.

In this paper, an integrated MEMS sensor, which is integrated microheaters and temperature sensors, has been studied for boiling process research. Nucleate boiling has high heat transfer efficiency, so it has been widely used in engineering [11-14]. Because the boiling process has a great heat transfer capacity due to the release of latent heat of phase change, whether in normal or in microgravity. However, the boiling process is also a very complex and illusory process, and its theoretical research has not yet reached a consensus [14-19]. By using a local pulse overheating method in the experimental mode of single bubble boiling, film microheater has been designed to excite bubbles. Under the control of the sensor, a bubble nucleus can be excited with accurate spatial and temporal positioning on the top-side of the microchip and meanwhile the local wall temperature around the bubble in boiling of water will be measured.

Although there are some literatures reports on the use of MEMS sensors [14-20], the theoretical research and the fabrication of these sensors and the characteristics of Ti/Pt films with a total thickness which is less than 100 nm are rarely reported in the literature. Therefore, this MEMS sensor has been studied in detail. Firstly, to analyze the

feasibility of the sensor, a model has been created to simulate the temperature and stress in different state by Finite Element Method Analysis. Then a microheater has been discussed in detail. Unfortunately, few papers discuss in detail the properties of ultrathin materials, which are critical for microheater performance prediction. Temperature changes in resistivity of thin-film materials are also often ignored. It should be noted that these are key material properties required for any thin film microheater modeling. The microheater used in this sensor, is also useful for short temperature pulse applications, like micro-thruster ignition and micro explosive boiling. Therefore, the discussion of thin film materials is of great significance. And then this senor was made on a bulk Pyrex substrate, which is furthermore compatible with harsh environments, and its lower thermal conductivity and higher electrical resistivity compared to silicon, enabling good thermal confinement and low power consumption. For heating circuits in general, detachment of the resistive layer often determines the failure rate. In working condition, excessive interfacial stresses thermally induced [15-16]. However, it is also easy to cause interfacial stress due to excessive heat, resulting in the detachment of the resistance layer. Once the layers are separated, it locally overheats, which will accelerate the separation. In the worst case, the circuit could overheat and burn out. So, the Thermal cycling experiment has been made to make sure the reliability of the sensor. All of the above issues will be discussed and analyzed in the following content.

II.   EXPERIMENTL PROCEDURE

A.   Method of the MEMS sensor

By using a local pulse overheating method, a microheater has been designed to excite a bubble nucleus with accurate spatial and temporal positioning on the top-side of the microchip. Several thin film micro-RTDs are used for precise temperature measurements on the heating surface around and underneath the growing bubble. And a main heater has been fabricated on bottom of the chip by using a double-sided photolithography process to keep the temperature of the entire device in a stable state. So, an integrated chip with micro-heater and micro-RTDs has been designed. And then a Pyrex-7740 glass is selected as the bulk substrate of the microheater because of its lower thermal conductivity and higher electrical resistivity compares to silicon, thus achieving good heat confinement and low power consumption. Fig.1(a) shows the principle of the microchip. Fig.1(b) shows the schematic of the microchip. Chip A integrates micro-heaters and micro-RTDs, chip B integrates micro-RTDs and a main heater.
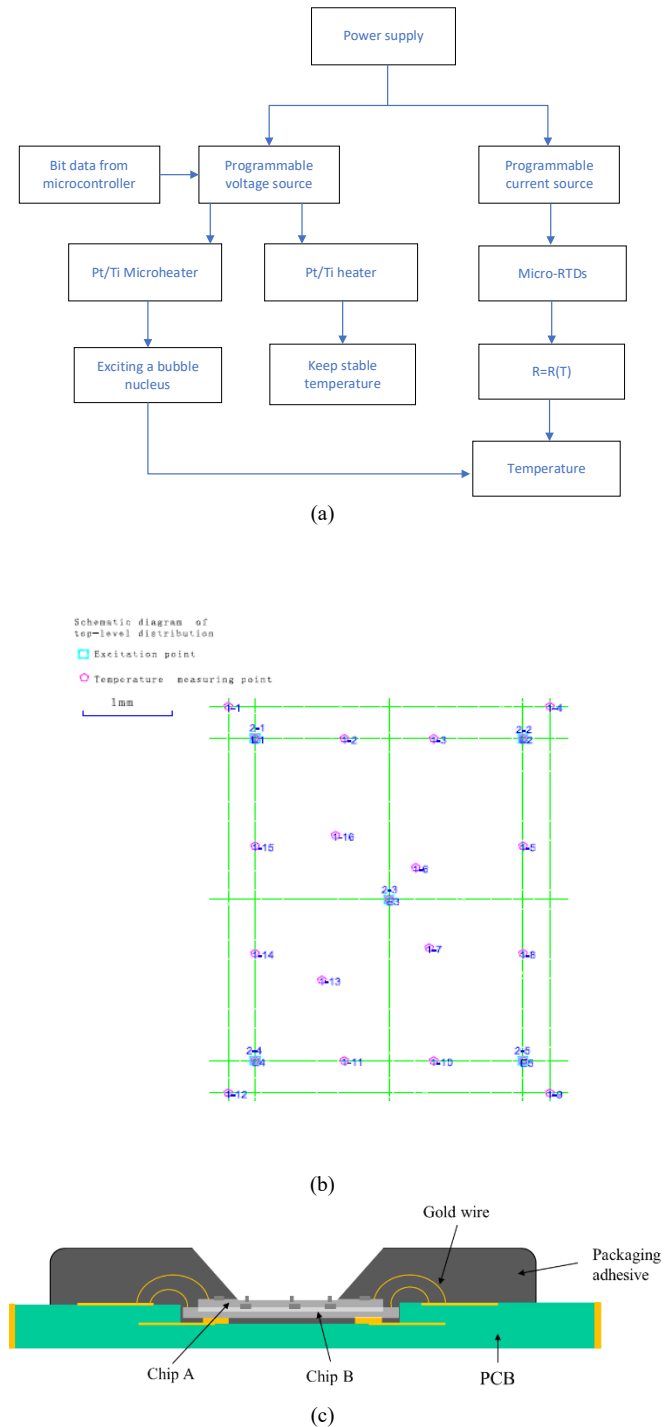

(a)

(b)

(c)

Fig. 1. (a) Principle of the microchip; (b)the layout of the chip excitation and temperature test point; (c) the schematic of the microchip.

After chips have been fabricated, a kind of plastic package, COB (chip on board) encapsulation, is used to encapsulate chip A and B as an independent electronic component. A PCB of 1.6mm in thickness is used to provide electric connections and mechanical support for the integrated micro heater. First of all, chip A and chip B are

bonded together by transparent epoxy resin, and the alignment error is less than 5um. And then the main heater is welded on the lower PCB by using the surface mount method, while the bubble trigger and local temperature sensors are bridge-connected with the upper PCB by double gold wires with a diameter of 25μm. 4 pins are connected with each end of the main heater on the back-side of the substrate for a good reliability, while only one pin is connected with each pad on the top-side. Finally, the substrate, as well as all gold wires, is packaged on the PCBs by using the packaging adhesive DOVER DE108.

B.   The simulation and the process of the MEMS microchip

We carried out simulations to better understand their influence on the bubble nucleus excitation so that the models can be further optimized. In order to simplify the simulation data, only the micro-heater and main heater have been modeled, as shown in Fig.2. To make sure the chip would not move randomly, we set it to rigid motion suppression. The chip works in a process fluid (309 K), we modeled the heat fluxes to the surroundings using heat transfer coefficients, h. On the glass plate's back side, which is not in direct contact with the liquid and has a large thermal resistance, assume h=20 W/(m²·K), representing normal convective heat transfer to the fluid. While on the front side, the equivalent heat transfer coefficient can be regarded as constant, h=70 W/(m²·K), which is calculated by the genetic algorithm inversion. [17]. Figure 2 shows a temperature distribution of the microchip model with 2V voltage. From the temperature distribution, we can get that the main heater can effectively keep the working area of the chip working area at a stable temperature, and the highest temperature is 374K, which is enough to prove the microheater realizes the necessary temperature rise. .
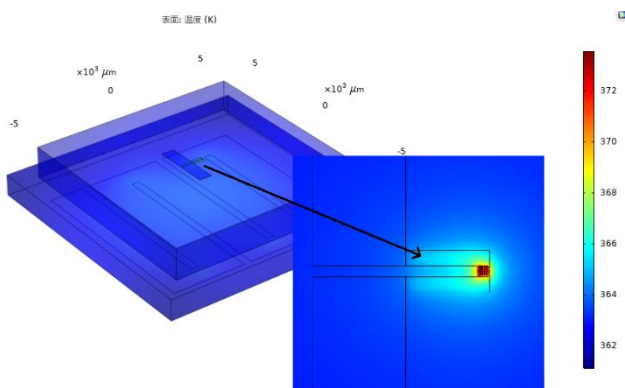

Fig. 2. FEM simulation of microheaterswith isometric view of the temperature distribution of the micro heater.

The integrated micro heater is fabricated by using CMOS technique. The fabrication process steps are presented in Figure 3 To facilitate good adhesion of a Pt layer, a Ti prime layer was first sputtered followed by the deposition of a Pt layer. A lift-off step was performed to remove the metal with a photoresist layer beneath. The thickness of the prime Ti and Pt layers was 10 and 35nm, respectively.

And then 400nm Au film was deposited by the same process. For the Chip B, on the back-side of the substrate, the main heater on the other side, double-sided alignment was utilized.

Considering size of the micro-bubble, the size area of the micro heater and the temperature sensor have been controlled in 65*65μm. And for the sake of safety, the bubble trigger is composed of two parallel serpentine strip of platinum film. Since the fluctuation of the surface is easily lead to the movement of bubbles, and this phenomenon has also occurred in our previous experiments, the surface of the microchip should be as smooth as possible. In this paper, the thickness of the metal film is designed to be 40nm. However, the application of the ultra-thin Ti/Pt film is rarely reported in the literature, which propose a new challenge for the application and reliability of the chip. So, the characteristic of the ultra-thin Ti/Pt film has been detailly discussed in the next chapters.
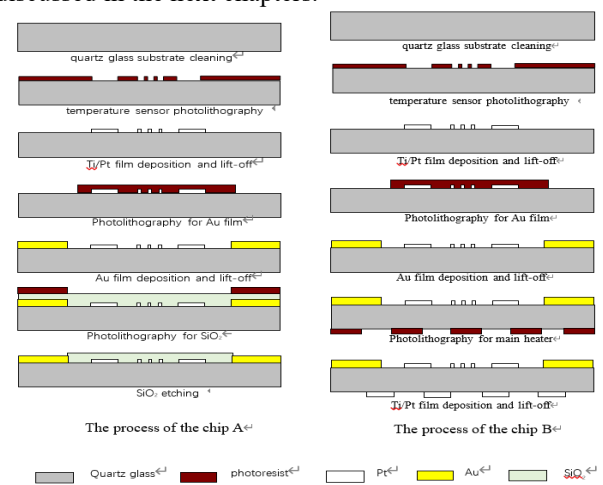

Fig. 3. The process of chip A and chip B.

C.   Ti/Pt film

As the thickness of the Pt film becomes thinner, its performance will change significantly [9,10, 24,25]. And it should be noted that these are key to the microchip. The large discrepancy in specific resistivity is attributed to the specific deposition method of the Ti/Pt layer and target purity, annealing ambient effects, layer thickness tolerance, the influence of a Ti-Pt interdiffusion and/or its interaction with the substrate layer. However, the characteristics of Ti/Pt film which is thinner than 100nm are seldom reported in the literature. Since the values of residual stresses in the Pt/Ti thin films deposited by magnetron sputtering and further thermal treatment were found to be more than 1.5 times lower comparing with the results obtained by other researchers [10]. Annealing the Ti/Pt film can not only reduce the stress but also improve its reliability [9,10,26]. Figure 4 shows the SEM image of the Pt film surface with different annealing temperature. It can be seen that the surface also presents different morphology as the annealing temperature increases. As the annealing temperature increases, the roughness of the metal surface also increases,

especially when the annealing temperature over 500°C, hillocks appeared on the heater surface. According to literature reports, when hillocks begin to appear on the surface of Pt film, the reliability of the device will also be affected [28,29]. Considering the thickness of the Ti/Pt (10/30nm) film and the maximum temperature reached by the chip application will not exceed 300℃, two annealing temperatures of 300℃ and 350℃ has been discussed. In order to ensure the accuracy of the test, we use the probe to test the resistance of the same chip before and after annealing.
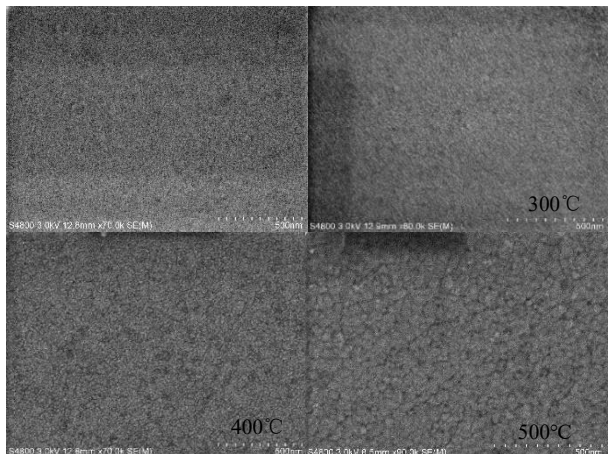
Fig. 4. The SEM image of the Pt film surface with different annealing temperature.

First of all, we compared the difference between rapid annealing and furnace tube annealing at different temperatures. Figure 5 shows the data of the chip resistance before and after annealing in the furnace tube for 1 and 2 hours, and 5 resistances were taken from each chip. We can get that the resistance is reduced by 5% after annealing at 300°C, and the resistance is reduced by nearly15% after annealing at 350°C. When the chip annealed for 1 hour is subjected to annealing for 2 hours, the resistance value remains unchanged. Figure 6 shows the result of rapid annealing for 5 minutes, after annealing at the same temperature, the rate of change is the same, and which is basically the same as furnace tube annealing. Therefore, we will choose to use rapid annealing in subsequent chip preparation.

And meanwhile a special phenomenon has been found during the experiments. As shown in the Figure 7, when there is a passivation layer SiO$_2$ on the surface, the resistance is reduced by 13% after annealing at 300°C, while the resistance is reduced by 5% after annealing at 350°C for the film passivation layer. And the resistance is reduced by nearly 5 % after annealing at 300°C, while the resistance is reduced by nearly 15 % after annealing at 350°C for the film without passivation layer. And the reason for this phenomenon is because when the surface is covered with a passivation layer, it can be seen that Ti/Pt film is annealed in a vacuum environment, while without a passivation layer, it can be regarded as being annealed in a gas atmosphere.

This phenomenon and the reason are rarely reported in the previous literature, but we should pay attention to the actual preparation and application, and it is worthy of further study. And we also found that the effect of annealing on resistivity will be different when the film thickness is different, for example, after annealing at 300℃, the change of the resistivity of the Ti/Pt (20nm/150nm) [10], Ti/Pt (15nm/240nm) [27] is less than 2%.
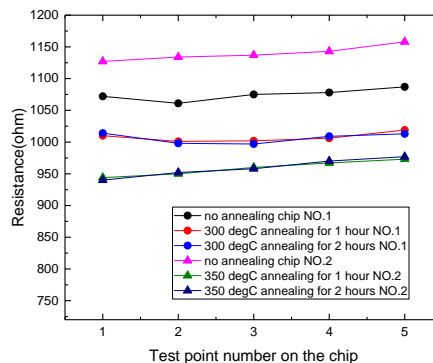

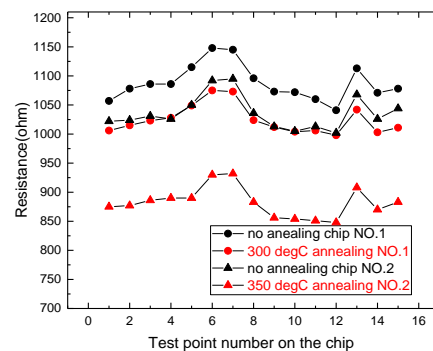Fig. 5. Ti/Pt film furnace tube annealing for 1 hour and 2 hours with 300℃ and 350℃.

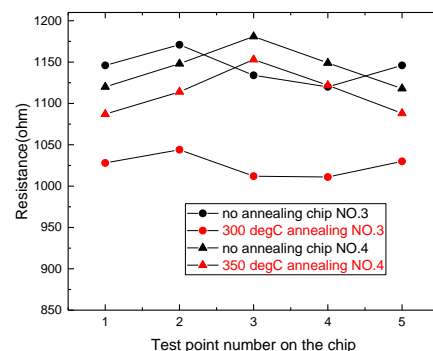Fig. 6. Ti/Pt film rapid annealing for 5min with 300℃ and 350℃.

Fig. 7. Ti/Pt film with rapid passivation layer SiO2 annealing for 5min.

D. *Thermal cycling experiment*

After the chip has been packaged, the thermal cycling experiments have been made to test its reliability. The experimental conditions are shown in the table1 below.

TABLE 1. Thermal cycling experiments condition

Temperature Range	-25℃～85℃
Temperature Variability	3～5℃/min
Dwell Time	4 Hours
High and low temperature start-up time	Start from high temperature
Cycles	13

Figure 8 shows the resistance values of the chip before and after the thermal cycle test. Since the liquid temperature in the boiling experiment is at low heat flux, and it will never be higher than 70°C, so the upper limit has been set to 85°C. It can be seen that after the thermal cycle test, all the resistors work normally and the average rate of change in resistance value is less than 0.12%, which is much smaller than the acceptable resistance change 1%. It can be obtained that this thin film microheater is stable and reliable.
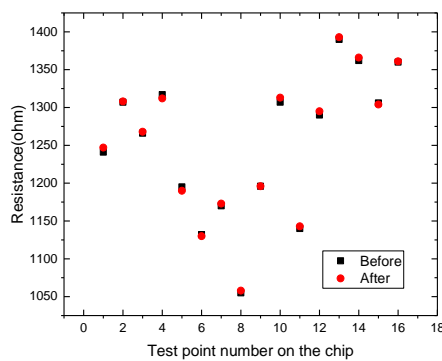

Fig. 8. The resistance of the chip before and after the thermal cycle test.

III. RESULTS AND DISCUSSION

Figure 9 shows the current and voltage curve of the microheaters, and the breakdown voltage is about 7V, which means that the microheater can work normally and stably when the normal pulse voltage is 0~5V. Figure 10 describes the temperature curve of resistance versus voltage at different temperatures, as well as the resistance versus temperature curve. According to these data, the temperature coefficient of resistance (TCR) of this Ti/Pt film can be calculated to be 0.19%.

Figure 11 shows the final top view of the two generation integrated chips, and the chip picture after packaging. As mentioned above, a 200nm -thick SiO_2 layer is covered on the top-side of the substrate of the integrated micro heater to protect the trigger and the local temperature sensors, as well as to smooth the heating surface. Thus, the

heater surface contacting directly with the working fluid can be well considered as an isotropic one with the same surface roughness and contact angle everywhere.
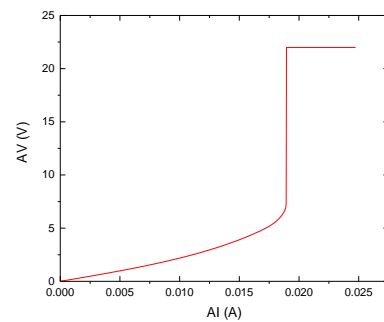

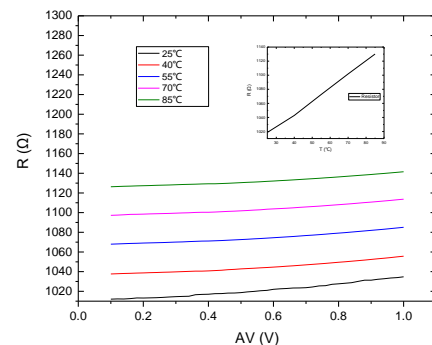Fig. 9. Pt/Ti micro heater voltage variation with current.

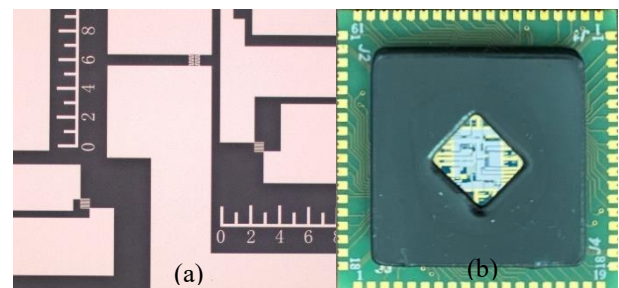Fig. 10. RTD resistance variation with voltage at different temperature

Fig. 11. (a) Top view of the two generation integrated chips. (b) Photograph of the integrated-chip after packaging.

Then the chip has been in the bubble excitation test, a boiling test with three different working modes was carried out with the preset liquid FC-76 temperature of 40°C and liquid FC-76 pressure of 100kPa. When the liquid temperature and pressure reached the preset values, the main heater was started to provide energy required for bubble growth.

Figure 12 shows the three working modes of the bubble exciter and the temperature values measured by the micro-RTDs. Among them, there are three bubble excitation modes, namely single bubble, asynchronous double bubble, and synchronous triple bubble excitation mode. Figure 13 shows the change of the bubbles with time. Due to the

effect of buoyancy, once the bubbles are generated, they will quickly break away from the heated wall. The bubbles have a short period, small size, and fast-moving speed (shown as a bright line in the image). From the above data and picture, our chip can normally work.
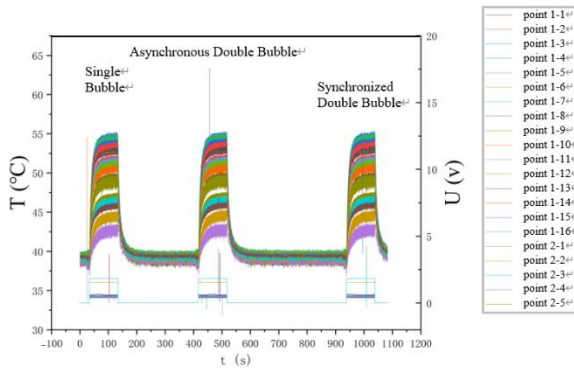

Fig. 12. Three working modes of the exciter and the temperature change law of the measuring point of the integrated micro-heater.
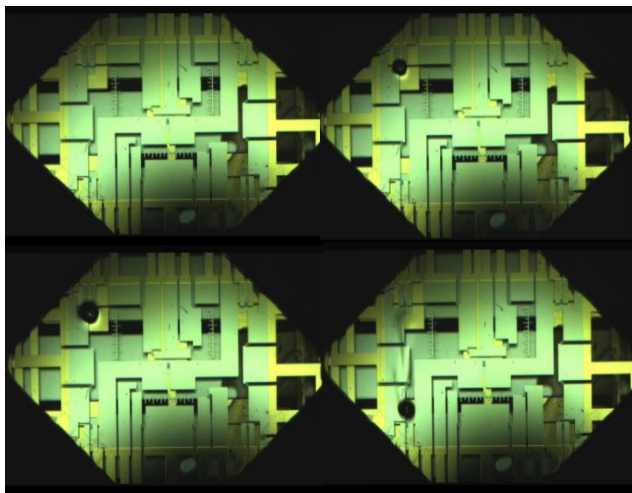

Fig. 13. Exciting point 2-1 (upper left) bubble changes over time on the earth.

Finally, the chip has been applied to SOBER-SJ10. After the Shijian-10 satellite was launched into orbit, SOBER-SJ10 completed the boiling experiment of the planned on-orbit phase for 15 hours at one time successfully. And after the recovery capsule was separated and returned, the ground experiment was successfully completed. The bubble excitation was successfully completed by controlling the chip, and the difference between the bubbles in the space and ground experiments was also successfully captured by the CCD.

Figure 14 shows the shape of the bubbles generated by the excitation of the microheater in the ground and space experiments. In the space experiment, the buoyancy is suppressed, and the bubbles are not easy to break away from the heated wall, will stick to the heating surface and grow, so it is spherical.

And it is also obtained that the shape of the growing

bubble and the temperature distribution below the bubble in normal gravity and microgravity.
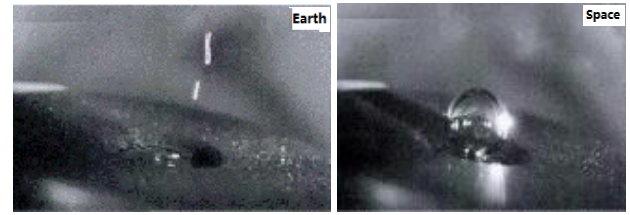

Fig. 14. Differences of bubbles in ground and experiments.

I. CONCLUSION

In this paper, an integrated microchip, which can help to reveal the characteristics of partial nucleate pool boiling heat transfer, has been designed, fabricated, simulated and tested. And the most important part, a thin film Ti/Pt microheater, has been studied detailly. And super thin Ti/Pt film has been studied in the process of the chip fabrication. The experimental data showed the electrical properties, morphology and residual stress of the Pt layers versus technological conditions. By thermal treatment and thermal cycling analysis of the Ti/Pt layer, it was found that thermal annealing had an effect on the resistivity of the Ti/Pt thin film layer, while thermal cycling would have no effect on the resistivity after the thermal treatment was completed. These also provided data support for deeper applications.

And the test results of microchip show that it works well as expected, and laid a good foundation for meeting the requirements of the future space experiments to obtain good data on pool boiling heat transfer in microgravity both in the single boiling mode and the normal pool boiling mode.

Data availability statement

All data that support the findings of this study are included within the article (and any supplementary files).

REFERENCEs

1   J. Puigcorbe, D. Vogel, B. Michel, A. et al, 2003 Thermal and mechanical analysis of micromachined gas sensors, Journal of Micromechanics and Microengineering 13 (5) 548–556

2   M. Baroncini, P. Placidi, G.C. Cardinali, A. Scorzoni, 2004 Thermal characterization of a microheater for micromachined gas sensors, Sensors and Actuators A 115 (1) 8–14

3   S. Glod, D. Poulikakos, Z. Zhao, G. Yadigaroglu, 2002 An investigation of microscale explosive vaporization of water on an ultra-thin Pt wire, International Journal of Heat and Mass Transfer 45 (2) 367–379.

4   K.L. Zhang, S.K. Chou, S.S. Ang, X.S. Tang, 2005 A MEMS-based solid propellant microthruster with Au/Ti microheater, Sensors and Actuators A 122 (1) 113–123.

5   Wu K, Li Z D, Zhao J F, et al. 2016 Partial nucleate pool boiling at low heat flux: preliminary ground test for SOBER-SJ10. Microgravity Sci Technol, 28: 165-178

6 Wu K, Zhao J F, Li H X, et al. 2017 Space and ground experiments on pool boiling phenomenon utilizing SOBER-SJ10 facility. J Eng Therm, 38: 2378-2381

7 Resnik D, Vrtacnik D, Mozek, M, et al. 2011 Experimental study of heat-treated thin film Ti/Pt heater and temperature sensor properties on a Si microfluidic platform. J. Micromech. Microeng. **21:** 025025

8 Gotz A, Gr acia I, Can and Lora-Tamayo E 1997 Thermal and mechanical aspects for designing micromachined low power gas sensors J. Micromech. Microeng. 7: 247–9

9 Puigcorbe J, Vogel D, Michel B, et al. 2003 High temperature degradation of Pt/Ti electrodes in micro-hotplate gas sensors. J. Micromech. Microeng. 13: S119-S124

10 Tiggelaar R M, Sanders R G, Groenlandc A W, et al. 2009 Stability of thin platinum films implemented in high-temperature microdevices. Sens. Actuators B, 152: 39-47

11 Moghaddam, S., Kiger, K. 2009 Physical mechanisms of heat transfer during single bubble nucleate boiling of FC-72 under saturation conditions I. experimental investigation. Int. J. Heat Mass Transf. 52, 1284–1294

12 Demiray, F, Kim J. 2004 Microscale heat transfer measurements during pool boiling of FC-72: effect of subcooling. Int. J. Heat Mass Transf. 47: 3257–3268

13 Siegele M, Gamauf C, Nemecek A, et al. Optimized integrated Micro-hotplates in CMOS technology. IEEE 2013 978-1-4799-0620-8

14 Myers, J G, Yerramilli, V K, Hussey, S W, et al. 2005 Time and space resolved wall temperature and heat flux measurements during nucleate boiling with constant heat flux boundary conditions. Int. J. Heat Mass Transf. 48: 2429–2442

15 Yabuki, T, Nakabeppu, O. 2014 Heat transfer mechanisms in isolated bubble boiling of water observed with MEMS sensor. Int. J. Heat Mass Transf. 76: 286–297

16 Yabuki, T, Hamaguchi, T, Nakabeppu, O. 2012 Interferometric measurement of the liquid-phase temperature field around an isolated boiling bubble. J. Therm. Sci. Technol. 7(3): 463–474

17 LIU Peng, DU Wangfang, ZHAO Jianfu, et al. 2021 Study on Performance of Pool Boiling Heat Transfer in SOBER-SJ10 Based on Genetic Algorithm, Journal of Engineering Thermophysics. Vol. 42(7): 1784-1790

18 DU Wangfang, LIU Peng, ZHAO Jianfu, et al. 2022 Boiling Water Aboard the China Space Station to Reveal the Gravity in Boiling Phenomenon. Mechanics in Engineering Vol. 3: 11-2064

19 ZS Lei，JF Zhao, et al. 2019 Numerical investigation of bubble dynamics and heat transfer in subcooling pool boiling under low gravity. International Journal of Heat and Mass Transfer 132: 1176-1186

20 Hu, W R, Zhao, J F, Long, M, et al. 2014 Space program SJ-10 of microgravity research. Microgravity Sci. Technol. 26: 159–169

21 Zhang, L, Li, Z D, Li, K, et al. 2015 Influence of heater thermal capacity on bubble dynamics and heat transfer in nucleate pool boiling. Appl. Therm. Eng. 88: 118–126

22 Li, Z D, Zhang L, Zhao J F, Li, H X, et al. 2015 Numerical simulation of bubble dynamics and heat transfer with transient thermal response of solid wall during pool boiling of FC-72. Int. J. Heat Mass Transf. 84: 409–418

23 Gao M, Zhang L X, Cheng P, et al. 2012 An investigation of microlayer beneath nucleation bubble by laser interferometric method. Int. J. Heat Mass Transf. 57: 183–189

24 Gerardi, C., Buongiorno, J., Hu, L., McKrell, T.: 2010 Study of bubble growth in water pool boiling through synchronized, infrared thermometry and high-speed video. Int. J. Heat Mass Transf. 53, 4185–4192

25 Sakaliūnienė J, Abakevičienė B, Šlapikas K, 2015 Influence of magnetron sputtering deposition conditions and thermal treatment on properties of platinum thin films for positive electrode– electrolyte–negative electrode structure. Thin Solid Films 594: 101-108

26 Chang I, Woo S, Lee M H, Shim J H, et al. 2013 Characterization of porous Pt films deposited via sputtering, Appl. Surf. Sci. 282: 463–466.

27 D. Resnik, J. Kovač, D. Vrtačnik, M.et al. 2017, Microstructural and electrical properties of heat-treated resistive Ti/Pt thin layers, Thin Solid Films, Vol. 639 64-72

28 H. Esch, G. Huyberechts, R. Mertens, et al. 2000 The stability of Pt heater and temperature sensing elements for silicon integrated tin oxide gas sensors. Sensors and Actuators B 65: 190–192.

29 H.N. Al-Shareef, K.D. Gifford, S.H. Rou, P, et al. 1993 Electrodes for ferroelectric thin films. Integrated Ferroelectrics Vol. 3: 321.